ISOPHOT POINT SOURCE CALIBRATION - WRAPPING IT UP

B. Schulz

ISO Data Centre, European Space Agency, Villafranca del Castillo, P.O. Box 50727, 28080 Madrid, Spain

ABSTRACT

The aperture photometer (PHT-P) and the FIR camera (PHT-C) of ISOPHOT were calibrated in-orbit using known point sources. Internal Fine Calibration Sources (FCS) provided a stable reference to correct for temporal drifts of the detector responsivities. This paper will review the principles of ISOPHOT calibration for staring and raster-mode observations, and summarise the treatment of instrumental effects. It will present the results and uncertainties derived from the final analysis that led to many of the calibration files in the final version of the automatic processing pipeline (OLP 10). This analysis is also used as a quality check for celestial calibrators. The discussion focuses on lessons for future missions.

Key words: ISOPHOT, calibration, data analysis

1. PRINCIPLE OF ISOPHOT CALIBRATION

The flux calibration of ISOPHOT (Lemke et al. 1996) on-board ESA's Infrared Space Observatory ISO (Kessler et al. 1996) is based on in-orbit observations of known celestial point sources like stars, asteroids and planets. The photoconductors used as infrared detectors are made from doped Silicon and Germanium. They exhibit a varying response to infrared radiation due to cosmic particle hits, but also as a result of the sequence of infrared fluxes seen before the actual measurement. Therefore highly reproducible internal IR sources (FCS) were used as secondary standards while the detectors acted only as comparators between the fluxes from the sky and the FCS. The FCS was calibrated over the full accessible flux range for each of the 25 filter bands, by observing calibration standards and the FCS at similar brightnesses. The emission by the FCS was adjusted to minimise the impact of signal transients that occur after a change of the illumination level. The adjustment of the FCS emission also reduced the influence of system non-linearities.

Once the FCS is calibrated, the detector responsivity R at a given time can be re-established with an FCS measurement via $R = I_{phot}/P_{fcs}(h)$, where I_{phot} is the measured photocurrent (without dark current) and P_{fcs} is the inband power received from the FCS, heated by the heating power h. The known R is then used in the same formula to determine the inband powers received from objects in the sky. This assumes that the relation between photo-current and inband power is strictly linear. In the case of ISOPHOT we faced a non-linear system, where many corrections had to be applied to the signal to make it proportional to the inband power.

In the following I will describe the derivation of both inputs to the formula, inband power and signal, then discuss the photometric effects and finally the accuracies.

2. INBAND POWER

Since system linearity could not be assumed a priori, standard sources had to be available for the entire dynamic range of all filters. The upper end of this range was limited by the maximum speed of the readout electronics and the current detector responsivity. The low end of the dynamic range was limited by either the dark current in the near-IR or by the celestial background from zodiacal light in the mid-IR and the Galaxy in the far-IR. The effective dynamic range of the detector signal covered between 2 and almost 5 orders of magnitude.

At short wavelengths (3-30 μm) there is a good coverage by the stellar SEDs provided by Cohen et al. (1996) and Hammersley et al. (1998), which have uncertainties of about 6 %. Only the brightest ones could be extrapolated to long wavelengths (40-200 μm) via Engelke functions with an accuracy of 10 %. The bright part of the dynamic range is covered by the planets Uranus and Neptune. From comparisons of model SEDs of different authors an accuracy of 10 % is adopted in the long wavelength range. To stay consistent with the Long Wavelength Spectrometer (LWS) on board ISO, the SEDs provided before by Abbas (priv. comm.) were replaced by the ones of Griffin & Orton (1993). The intermediate flux range at long wavelengths was filled by asteroids. These objects posed some additional difficulties for modelling and scheduling of observations due to their variability and proper motion. The models provided by Müller & Lagerros (1998), achieved an accuracy of 10 % for most of the observed objects.

The inband power for a given filter and a given calibrator is then calculated as the integral over all wavelengths of the product of the source SED, the known spectral filter transmissions and the relative spectral response function of the detector, times the telescope collecting area and the PSF-correction factor $f_{PSF_{f,a}}$. See Schulz et al. (1999) for more details on inband power calculation and source lists.

3. SIGNAL CONDITIONING

To derive a detector signal that is consistent with a linear system, i.e. where the flux dependent part of the signal is propor-

Proceedings of the Conference "The Calibration Legacy of the ISO Mission", VilSpa, Spain, February 2001
ESA SP-481, 2003, eds. L. Metcalfe, A. Salama, S. B. Peschke & M. F. Kessler

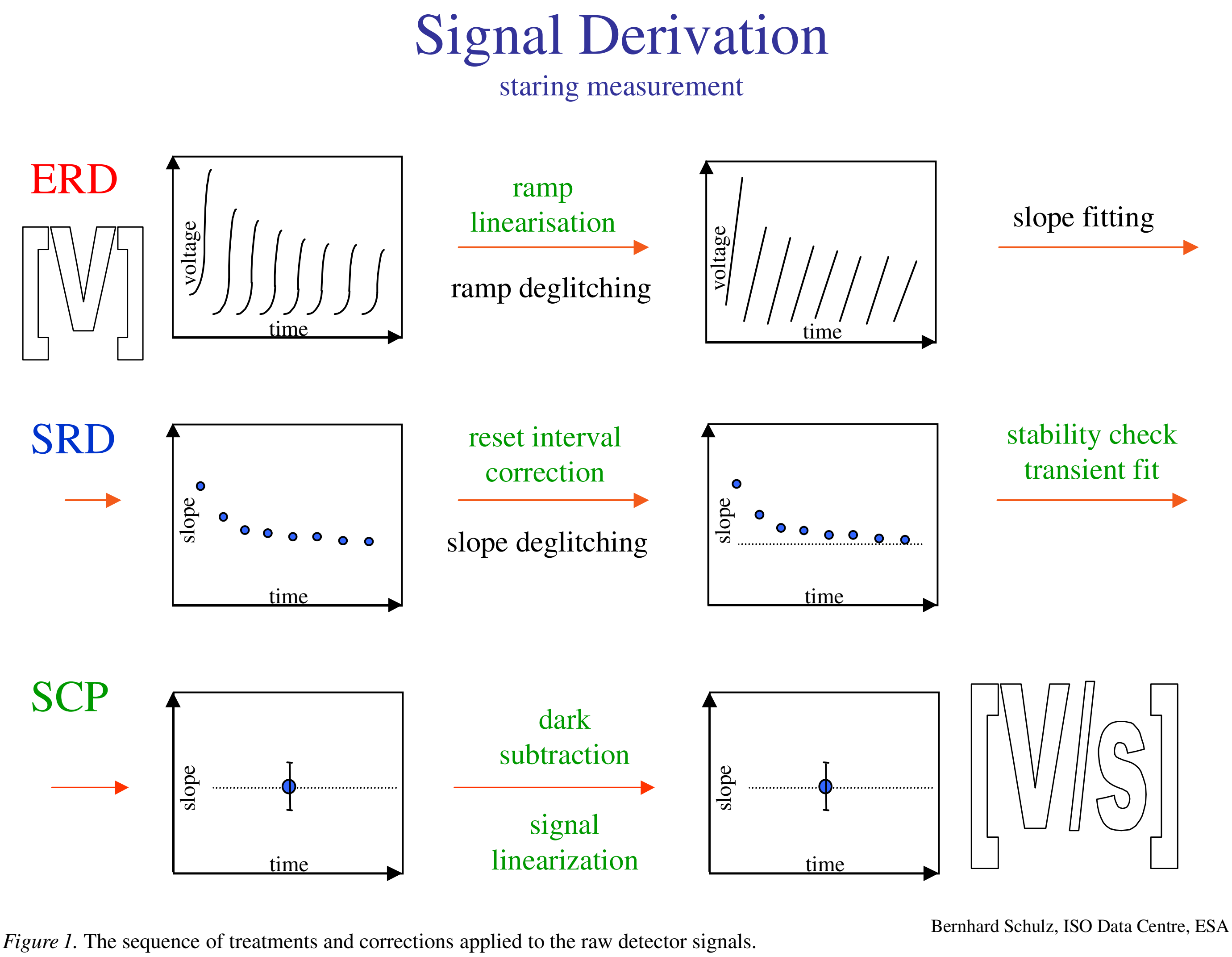

Figure 1. The sequence of treatments and corrections applied to the raw detector signals.

tional to the flux, a number of corrections are necessary. In the following I will give a brief description of the reduction steps while adhering to the nomenclature of the PHT Interactive Analysis (PIA) (Gabriel et al. 1997). The extrinsic photoconductors used in ISOPHOT show very high resistances. The typical photo-currents are between 10^{-16} and 10^{-11} A. They charge a capacity inside an integrating cold readout electronics (CRE). The rising output voltage that is transmitted to the warm electronics outside the cryostat is proportional to the accumulated charge. Intermittent discharging of the capacitor via a "reset-switch" before hitting the saturation limit of the amplifier, creates a continuous series of integration ramps. Their slope, which will be referred to as 'signal', is ideally proportional to the photo-current, which in turn should be proportional to the inband power. The data corresponds to the primary level, called Edited Raw Data (ERD).

In practice these integration ramps deviate from the ideal straight line. This ramp non-linearity was found to depend on the absolute output voltage of the CRE. Calibration tables were derived for linearisation.

Each integration ramp is formed by a number of discrete readouts. Hits of the detector by cosmic particles increase the photocurrent momentarily, so that the slope between the previous and the next readout is larger than the average (glitch). In a first deglitching stage, these excess slopes are detected and the affected integration ramps are "repaired". The algorithm also tries to catch small transients, that occur sometimes after the main hit.

Fitting of straight lines to the ramps to determine their slope marks the transition to the next data level called Signal per Ramp Data (SRD). Here a second procedure to eliminate glitches is applied (see Gabriel et al. 1997).

After a change of flux, the signal follows a complex path called transient, which eventually settles asymptotically at the new equilibrium value S_∞. Time constants are of the order of seconds and minutes, depending on the flux level. To determine S_∞, two cases have to be distinguished, depending on whether the signal has stabilised within the measurement time or not.

For the automatic reduction of the FCS calibration data we used a non-parametric statistical test (Mann-Test) to determine if a sufficiently long and stable interval at the end of the mea-

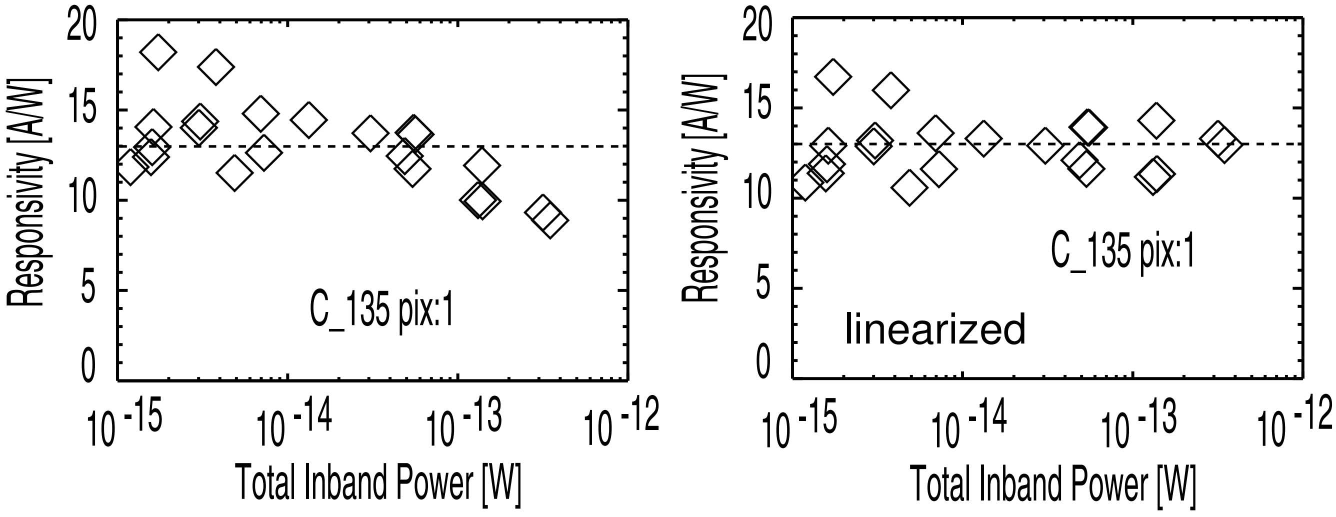

Figure 2. Responsivities depending on inband power before and after signal linearisation.

surement could be found. The average of this interval provides the best estimate for the equilibrium signal. If the measurement did not stabilise, an empirical transient model was used to estimate the final signal, since no physical models are available yet that describe the effect with sufficient accuracy and that can be practically used. Our transient model is of the form $S(t) = S_\infty + (S_0 - S_\infty)e^{-ct}$, where S_0 is the signal before the flux change and c is a free fit parameter. It is quite successful, although a rigorous quality check had to be developed to reject unreliable solutions (Huth & Schulz 1998). Accepted solutions deliver corrections of up to 30 %. The best estimates for S_∞ for each interval of constant flux represent the Signal per Chopper Plateau (SCP) level of data reduction.

We found that the signal derived from a constant celestial source is not independent of the choice of the operating parameters of the CRE. In particular the reset interval (time between two resets of the integrating capacitor) can cause changes of the derived signal by up to 40 % relative to the maximum. In a dedicated programme constant celestial sources were measured in all generally used configurations of the CRE. The results were translated into correction tables that can be applied either at SRD or SCP level.

After subtraction of the dark signal, which is tabulated depending on the time within the revolution, and after correction for the periodic orbit dependent variations, R should be statistically distributed around a constant due to its remaining variability with time. The left diagram of Figure 2 shows R of the C_135 filter revealing a clear dependence on the inband power. Similar dependencies have been found for all filters. We derived correction tables for the signal in such a way that the responsivities become statistically signal independent (see right diagram). Great care had to be taken not to overinterpret the sometimes very few and scattered data points.

4. PHOTOMETRIC CORRECTIONS

The relations between FCS heating powers h and resulting inband powers P radiated onto detector pixels form the so called FCS power curves $P_{fcs_f}(h)$. These were established from the measurements of sky calibrators individually for each of the 25 filter bands and each FCS. Each FCS contained a bright and a faint radiator (TRS 1 and 2), which were dedicated to the short wavelength detectors (P1, P2) and the long wavelength detectors (P3, C100, C200) respectively. Due to a change of the radiation characteristics of TRS 2 of FCS1 after revolution 93, the curves for P3, C100 and C200 had to be determined again, bringing the total number of power curves to $25+25+13 = 63$. In the early phase, when only few measurements were available, the power curves were established by fitting a Grey-Body model to the data. Now the power range covered by measurements is interpolated by polynomials, while the model is still used to extrapolate the curve.

The FCS was designed to illuminate the C-detectors uniformly. In reality there are small differences between detector pixels. These patterns vary for different filters and are corrected via "illumination" matrices $\Gamma_{p,f}$, assuming the effect to remain achromatic. Similar effects seem to appear in the aperture photometer P, however the large number of possible combinations of filters and apertures, the pronounced drifts induced by flux changes and the unusual beam profiles have prevented so far a good understanding of aperture/filter combinations other than the standard ones ($23''$ for filters P_3.29. . . P_7.7, $52''$ for P_10. . . P_16, $79''$ for P2 and $180''$ for P3). For the time being the calibration presented here applies only for these standard combinations. Deviating combinations suffer from increasing systematic errors.

After including the relative spectral response into the inband power calculation, R should be independent of filter. Measurements of filter sequences on calibration sources within time intervals of stable responsivity showed still different responsivities between filters. The pattern is independent of the source within an uncertainty of about 10 %. P1 shows a wavelength dependence, where the longest wavelengths apparently loose flux of almost 70 % compared to the shortest wavelengths. The large effect is not understood. We can only speculate that this is related to the design of the cavity and perhaps due to spectral absorption of materials inside the cavity (sapphire substrate, glue). The other detectors show maximum losses of 50 % compared to the filter with the brightest responsivity. These effects are less correlated to wavelength. The inhomogeneity across pixels is interpreted in terms of projections of spatial inhomogeneities of filters, which are mounted not in the pupil of the beam but close to the detector arrays.

Factors $\chi_{p,f}$ are derived from these observations, which correct the fluxes so that the measured responsivity becomes independent of the filter. The applicable formal error of 10 % only needs to be included for multi-filter observations, where the FCS measurement is performed in a different filter than the sky observation.

We can write now a set of formulae to calibrate observations with ISOPHOT. First, the detector responsivity is determined from the FCS-measurement using

$$R_p = \frac{(S_{fcs_{p,f}} - S_{str_{p,f}})C_{int}}{P_{fcs_f}(h)\Gamma_{p,f}\chi_{p,f}}. \tag{1}$$

$S_{fcs_{p,f}}$ is the FCS signal and C_{int} is the integration capacity of the CRE. The indices p,f,a designate dependencies of pixel, filter and aperture respectively. The FCS Straylight signal $S_{str_{p,f}}$ was measured directly only in absolute photometry AOTs and in dedicated FCS calibration measurements. In all other cases it is replaced by the orbit dependent dark signal. In the second step, the in-band powers, Φ_f, for the sky measurements are calculated as

$$\Phi_{p,f} = \frac{S_{src_{p,f}}C_{int}}{R_p\chi_{p,f}}. \tag{2}$$

The transformation into a flux density, F_ν, at the reference-wavelength of the filter is performed by

$$F_{\nu_{p,f}} = \frac{\Phi_{p,f}}{C1_f\ f_{PSF_{f,a}}} \tag{3}$$

where $C1$ is a filter dependent constant.

5. CONSISTENCY AND ACHIEVABLE ACCURACY

The instrument stability was verified using fainter and brighter non-variable celestial sources. From revolution 503 on we performed monitoring measurements, every 2 weeks on faint stars and every 5 weeks on the bright planetary nebula NGC6543 in the standard filters of each of the 5 photometric subsystems. The results are given in Table 1. The fainter sources show a larger scatter due to bigger uncertainties in the background. The influence of glitches and transients is greater at low fluxes. The bright source measurements show reproducibilities far better than 10 %.

Table 1. Results of the monitoring programme of faint and bright fluxes. The columns show source name, filter, aperture, flux from model-SED, measured error weighted average flux and standard deviation.

source	filter	apert.	F_ν [Jy]	$F_{\nu_{meas.}}$ [Jy]	σ [%]
HD172323	P_11.5	52″	0.085	0.087	10.0
HR5986	P_25	79″	0.667	0.588	12.3
HR7310	P_60	180″	0.667	0.574	7.0
HR7310	C_100	-	0.229	0.250	10.6
HR6705	C_160	-	0.672	0.631	7.2
NGC6543	P_11.5	52″	–	6.8	5.9
NGC6543	P_25	79″	–	107	1.8
NGC6543	P_60	180″	–	144	6.6
NGC6543	C_100	-	–	59.5	2.0
NGC6543	C_160	-	–	15.9	2.6

To assess the overall accuracy of the instrument, a complete error propagation through all reduction steps is very difficult and, due to the many observing modes and possibilities to combine single measurements, impractical. Instead the accuracy is estimated from the consistency of the FCS power curves and the data points they were derived from. Consequently each data point includes all systematic and random error contributions that would also apply for any other astronomical observation in staring or raster mode. Note that measurement times on average were longer for calibration measurements (64-256 s), so there might be small biases compared to short measurements with imperfect transient correction. The ratios of FCS power curves and measurements are plotted against the FCS heating power as an indicator of flux regime (see Figure 3). More noise is found at lower fluxes. Depending on the detector subsystem, 1 σ accuracies of 7 to 18 % were found for the high flux part and 11 to 25 % for the low flux part.

The same dataset was used to analyse the consistency among calibration sources. In Table 2 I note the average biases, the standard deviation and the number of data points individually for each source. The long and short wavelength regions are separated too. Sources with total biases above 10 % are emphasised in bold letters.

The interpretation of this table is however not straight forward due to the entanglement of systematic and statistical errors. Uranus and Neptune for instance will never show biases because their fluxes are too different from other standards. Also the biases seen in fainter standards such as HD172323 and HD184400 should not be overinterpreted, since uncertainties increase for low fluxes.

However, the data still can provide clues about sources that deviate from the general picture, when enough measurements of other standards are available within the immediate flux neighbourhood. HR7001 (Vega) is a good test case, where the observed bias is consistent with the well known excess. HR3748 (α Hya) and HR6514 stick out below 30 μm, however α Hya shows no considerable bias at longer wavelengths. The biases

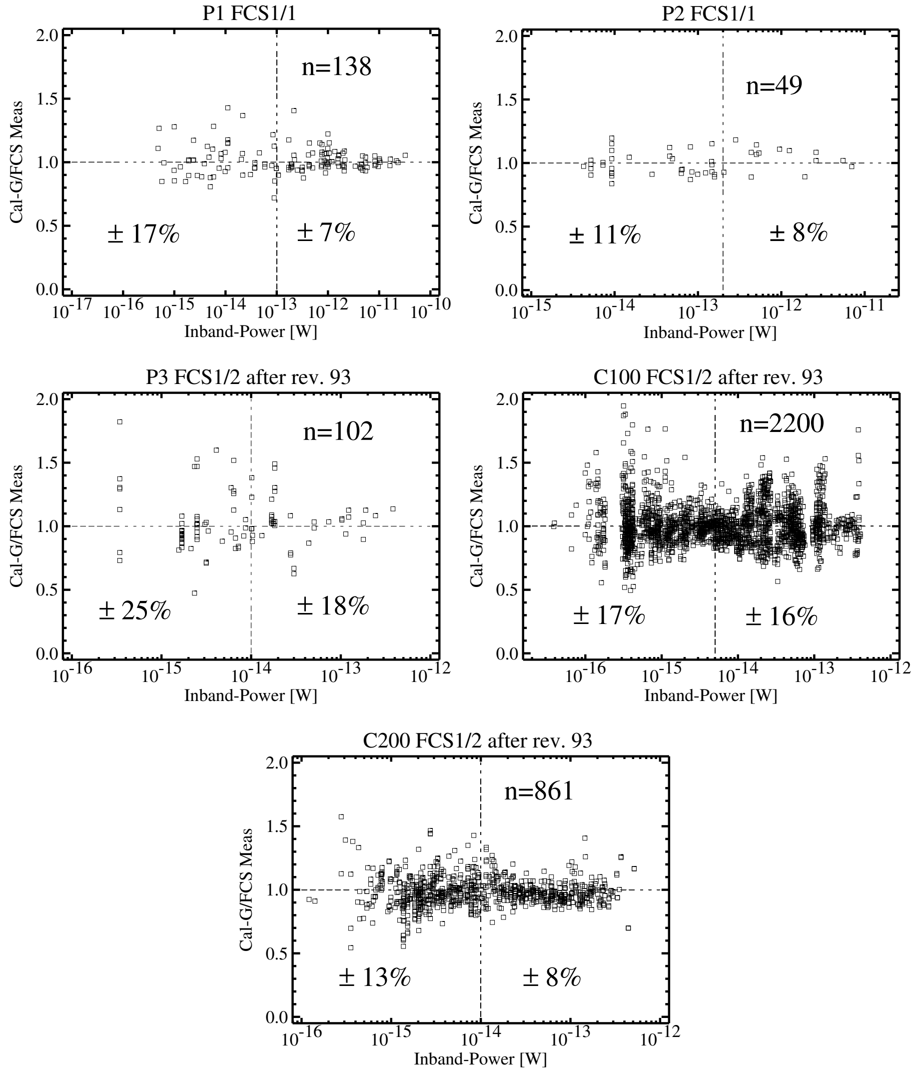

Figure 3. Consistency of FCS power curves and measurements they were derived from.

found for β And and HR7633 at long wavelengths are more likely to be indicators of dust emission around these objects.

6. DISCUSSION

With the last version of the pipeline processing, the point source calibration in staring mode and P03/P22 mapping modes is consolidated. Many effects, not included in the standard instrument model, had to be investigated and corrected for. The aperture photometer with its large number of configurations is best calibrated for the standard aperture/filter combinations. The photometric reproducibility over 550 days was better than 10 % and the self consistency of the calibration data suggests photometric accuracies of 10-25 %, depending on detector type

Given that other challenging missions like SIRTF or Herschel are ahead and may still benefit from our experience, it is useful to take a step back and look at some of the lessons learned. I will do this here by discussing in hindsight some improvements that I would introduce, if the same mission was to be flown again. This exercise must be understood strictly in the context of looking back at a mission, at a time when a complex learning process was completed and interrelations become clear that were not obvious before. For consistency I will disregard new technical developments that would be available today.

First of all, the number of possible instrument configurations would have to be reduced drastically for a mission duration of only 16 months. Our experience shows that each configuration needs to be measured and verified at least once. It turned out to be dangerous to rely on future instrument modelling to cover regions of the parameter space that can not be verified by actual measurements due to time limitations. The PHT-P beam profiles that deviated considerably from expectations are such an example.

An adequate reduction of instrument configurations would be achievable by removing the aperture photometer PHT-P, which

Table 2. Individual biases of sources in per cent from a consistency analysis of measurements of calibration standards.

$3\ldots30\mu m$				$30\ldots240\mu m$			
source	bias %	σ %	n	source	bias %	σ %	n
HR0337	-2	7	8	β And	**12**	**24**	**16**
HR0617	-1	9	12	α Ari	5	18	8
HR5340	3	8	26	α Boo	-5	11	295
				ω Cap	9	22	125
HR6705	5	10	38	γ Dra	-2	14	269
HR3748	**14**	**-**	**1**	α Hya	3	9	129
				ϵ Lep	5	14	144
HR8775	9	8	16	β Peg	6	8	116
				α Tau	4	22	19
				HR6688	2	12	20
HR7310	4	9	17	HR7310	8	23	373
HR7633	0	12	8	HR7633	**52**	**16**	**8**
HD172323	**18**	**30**	**12**	Ceres	2	17	321
HD184400	**16**	**24**	**8**	Pallas	3	15	264
HR5986	0	11	14	Juno	**11**	**10**	**139**
HR6514	**16**	**34**	**2**	Vesta	9	16	282
HR6847	8	2	2	Alexandra	-8	11	32
HR7001	**12**	**6**	**3**	Chaldaea	-5	23	143
HR7341	2	8	3	Cybele	6	11	152
HR7451	0	9	2	Dione	**20**	**19**	**160**
HR7469	-4	3	2	Herculina	**-12**	**13**	**201**
HR7742	-1	3	8	Hygiea	**13**	**20**	**241**
				Neptune	-2	15	364
				Uranus	3	10	179

has a large overlap in wavelength coverage with PHT-S, PHT-C and ISOCAM. This would eliminate not only the difficulties with the beam profiles of PHT-P, but also reduce the number of possible optical configurations by a factor of 14.

The number of FCS power curves to calibrate could be reduced by a factor of 5 by installing the FCS close to the detectors. Illuminating them diffusely instead of routing their radiation through the entire optical system eliminates the need to determine the curves for every filter/FCS combination separately.

The chopper mirror would be another item, that could be removed in order to reduce complexity. Problems encountered in ISOPHOT were i) dependencies of the photometry on the deflection angle and ii) loss of signal and S/N due to transients. Since each deflection angle constitutes another optical configuration, the chopper would boost the number of configurations to be calibrated. The measurement technique to be favoured instead would be the so called “nodding mode”, where the detector stays active while the telescope changes repeatedly between on- and off-source position but with much longer dwell times and no changes in the optical system. Instead a shutter would be a useful addition, to identify straylight components from outside of the instrument, especially at long wavelengths. To reduce the filter dependent spatial effects in the C-detectors, the position of the filters would have to be moved closer to the pupil.

Also the AOT design would have to be reviewed for another mission. Responsivity drifts were notable during all longer AOTs requiring corrections that were difficult to derive due to the lack of additional FCS measurements. The redundancy of measurement sequences would have to be increased considerably in order to enable correction of time dependent responsivity drifts to first and second order. For instance, repeated FCS flashes every minute and a nodding or mapping scheme could be considered here. Integrating the determination of the background into the AOT would not only help the achievable S/N but also facilitate any automatic processing afterwards.

It should be noted that most of these potential improvements, although some may appear now obvious, could only be stated with confidence during or after the mission, since only then the interplay of all components and effects could be studied. This once more emphasises the importance of extended integrated system tests already on the ground with realistic environmental simulations, sophisticated modelling and a close to final software environment. In particular the last two parts are often neglected due to lack of budget and time. However, it can not be stressed enough that not only noise performance, but also the photometry of such an instrument must be understood and mastered to considerable detail already before launch.

ACKNOWLEDGEMENTS

The author wants to thank the members of the ISOPHOT IDT and all providers of calibration standards for their support, and in particular R. Laureijs for valuable comments.

REFERENCES

Cohen, M. et al., 1996, AJ, 112, 2274

Gabriel, C. et al., 1997, Proc. of the ADASS VI conference, eds. Hunt, G. & Payne, H.E., 108

Hammersley, P. L. et al., 1998, A&AS, 128, 207

Huth, S. & Schulz, B., 1998, ASP Conf. Ser. 145: ADASS VII, 7, 212

Kessler, M.F. et al., 1996, A&A, 315, L27

Lemke, D., Klaas, U. et al., 1996, A&A, 315, L64

Müller, T. & Lagerros, J., 1998, A&A, 338, 340-352

Schulz, B. et al., 1999, ESA SP-427, vol. 1

Griffin, M. J. & Orton, G. S., 1993, Icarus, 105, 537